Competitive processes in the associative ionization of C^- with C^+, N^+, and O^+

A. Le Padellec
Université de Toulouse; UPS; CESR; 9 avenue du Colonel Roche, F-31028 Toulouse Cedex 9, France and CNRS; UMR5187; F-31028 Toulouse, France

J. Liévin
Service de Chimie Quantique et Photophysique, Université Libre de Bruxelles, CPi 160/09, 50 avenue F.D. Roosevelt, B-1050 Brussels, Belgium

E. M. Staicu-Casagrande
LCAM, Université Paris-Sud, Bâtiment 351, 91405 Orsay Cedex, France

T. Nzeyimana, E. A. Naji, and X. Urbain
Unité PAMO, Département de Physique, Université Catholique de Louvain, Chemin du cyclotron 2, 1348 Louvain la Neuve, Belgium
(Received 20 June 2008; published 4 December 2008)

Absolute integral cross sections have been measured for associative ionization reactions involving the C^- and C^+, N^+, and O^+ reactants. These measurements, obtained using a merged-beam setup in the keV range, provide us with useful experimental information on the efficiency and mechanisms of molecular ion formation from ionic reactants. The relative magnitudes of the different cross sections are rationalized by considering the spin multiplicities of initial and final states, and the exothermicities of the detachment and transfer ionization channels. The very different production efficiencies of CO^+ ions via the O^-+C^+ and C^-+O^+ channels are explained by statistical and energetic considerations. The potential energy curves of CO and CO^+ have been calculated by quantum *ab initio* methods in order to characterize the reactive pathways leading to autoionization. Thermal rate coefficients are derived to serve the plasma physics community.

DOI: 10.1103/PhysRevA.78.062705 PACS number(s): 34.50.−s, 82.30.Nr, 31.10.+z, 95.30.Ft

I. INTRODUCTION

The radiative association (RA) and associative ionization (AI) processes are two obvious formation mechanisms of molecules in binary collisions. The former leads to a charged or neutral molecule together with the emission of a uv photon, and usually occurs with a weak integral cross section due to the large amount of energy brought into the molecular complex. The latter leads to a molecular cation together with an electron, and is efficient since autoionization occurs in the time scale of the collision. It is often endothermic from ground-state neutral reactants, while it is usually exothermic from charged reactants. Before presenting our data, we shall make several points concerning the molecular products under scrutiny.

The C_2 molecule is found in a wide variety of astrophysical objects, ranging from comets, interstellar clouds, to the atmosphere of carbon stars [1–3]. At present, no evidence has been found for its cationic counterpart, i.e., the dicarbide ion C_2^+, though it is considered in the UMIST database for astrochemistry as the product of the $C^+ + C$ radiative association reaction. The cyanogen ion CN^+ is also not reported in interstellar clouds, though again it is considered in the UMIST database, despite neutral cyanogen being one of the first molecules to be detected [4]. A possible explanation for this nondetection is that the C_2^+ and CN^+ radicals are very efficiently removed by a wide range of ion-molecule reactions. Carbon monoxide cation CO^+ is the only molecular cation of the three that has been detected in the interstellar medium so far, though it is not plentiful at the interfaces between molecular clouds and HII regions around massive O stars [5,6] where it is removed by fast conversion of CO^+ into HCO^+ by reaction with H_2. On the other hand, CO^+ usually has significant abundance in the hot layers of photon-dominated regions (called PDRs), where a significant fraction of hydrogen is present in atomic form.

As a matter of fact, associative ionization reactions from charged reactants, namely, $C^- + C^+ \rightarrow C_2^+ + e^-$, $C^- + N^+ \rightarrow CN^+ + e^-$, and $C^- + O^+ \rightarrow CO^+ + e^-$, are not at all considered in reaction schemes and astrophysical databases, due to the weak abundance of the negative ions that are easily removed by radiation or charge exchange. Our point is that this undeniable fragility could somehow be balanced by the very large efficiency of the AI process, and therefore that this latter reaction should definitely be taken into account. Our communication is divided as follows. A brief description of the experimental setup is given first. It is followed by a presentation and a discussion of our results that are put in perspective with existing data. A conclusion is then drawn.

II. EXPERIMENTAL PROCEDURE AND SETUP

The merged-beam apparatus, pumped in high vacuum and divided into four sections, was described in Ref. [7]. The first section contains the ion sources, the mass selectors, and all the beam optics. We have replaced the duoplasmatron ion source with a high-intensity cesium-sputtering ion source in order to produce the negative ion beam C^-. The cationic beams were produced with an electron cyclotron resonance (ECR) source, and the C^+ cations on the one hand, N^+ and O^+ on the other hand, were produced from electron impact

dissociation of carbon monoxide and nitrous oxide, respectively. The two ionic beams are further merged in the second section. The third section, pumped in ultrahigh vacuum, corresponds to the (6.8 ± 0.2)-cm-long interaction region. The primary and product ion beams are deviated and their intensities recorded in the last section by means of a magnetic analyser. A cylindrical deflector guides the reaction products towards a channel electron multiplier to be counted. The following relation relates the number of events N that occur during the acquisition time T to the absolute integral cross section σ:

$$N(T) = \sigma \frac{v_r}{q_1 q_2 v_1 v_2} F \int I_1(t) I_2(t) dt, \qquad (1)$$

where v_r, v_1, v_2, q_1, q_2, I_1, I_2 represent the relative velocity, the beam velocities in the laboratory frame, their charges and their current, respectively. The so-called time-independent form factor F accounts for the degree of overlap of the two interacting beams. It is a nontrivial parameter to evaluate, but one might overcome this difficulty by making use of the core of the reactant beams. This collimation minimizes the effects of the angular and energetic dispersions. In addition to this, we have carried out detailed numerical simulations, which showed that the relative velocity distribution at 0 eV nominal energy follows a Maxwellian distribution, with an equivalent temperature of about 90 K. Therefore, due to the finite-energy resolution of our apparatus, we have restricted our data presentation to center-of-mass energies greater than 10 meV. The interaction length that enters the form factor is fixed by applying a bias voltage to a set of electrodes that simultaneously determine the interaction energy, as the ions speed up or slow down when entering the bias region, and allow for product discrimination.

III. RESULTS AND DISCUSSION

Two issues have first to be addressed: the electronic excitation of the primary ions and the internal excitation of the molecular products. We recall the conclusion of Ref. [7] concerning the singly positively charged primary ions since these have been produced with the same experimental protocol. We have populated the ^4P state in our carbon ion beam, in addition to the ^2P ground state [8]. Electronically excited $N^+(^1D, ^1S)$ [9] and $O^+(^2D)$ [10] cations were also present, in addition to the ^3P and ^4S ground states, respectively, but in unknown proportions. With regard to the negatively charged primary ions, the situation differs from the O^- case, the archetype of an anion with a unique bound state. The C^- ion has two bound states: the $^4S_{3/2}$ ground state and the ^2D metastable state, both arising from a $2p^3$ configuration [11,12]. Since the corresponding electron affinities relative to the parent $2p^3\ ^3P_0$ ground state are 1.26 eV and 0.033 eV, respectively, it is clear that the fragile ^2D metastable state would not have survived its time of flight up to the interaction region.

We now have to focus on the electronic and rovibrational excitation of the molecular products, C_2^+, CN^+, and CO^+. The situation with the electronic states of C_2^+ is rather complex, and is still a matter of some controversy due to the density of the electronic spectrum. Fourteen of these states can be populated at 0 eV: $X\ ^4\Sigma_g^-$, $a\ ^2\Pi_u$ (0.5 eV) [13], $A\ ^4\Pi_g$ (1.2 eV) [14], $b\ ^2\Delta_g$ (1.4 eV) [15], $c\ ^2\Sigma_g^+$ (1.7 eV) [16], $d\ ^2\Sigma_g^-$ (1.8 eV) [15], $e\ ^2\Pi_u$ (1.9 eV) [16], $B\ ^4\Sigma_u^-$ (2.4 eV) [17], $f\ ^2\Pi_g$ (2.9 eV), $C\ ^4\Delta_u$ (3.4 eV), $D\ ^4\Sigma_u^+$ (3.5 eV), $g\ ^2\Sigma_u^+$ (3.6 eV), $h\ ^2\Sigma_u^-$ (3.7 eV), and $i\ ^2\Delta_u$ (4.3 eV) [15].

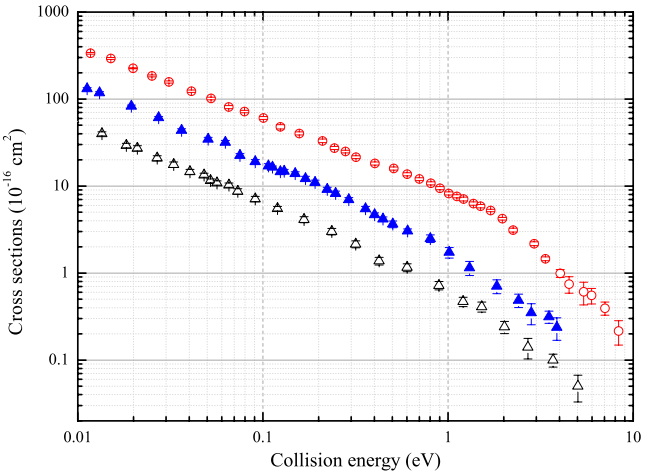

FIG. 1. (Color online) Integral cross sections for the associative ionization process along the C^-+C^+ channel (open circles), along the C^-+N^+ channel (full triangles) and along the C^-+O^+ channel (open triangles).

As for C_2^+, the situation with the electronic states of CN^+ is also rather complex: the assignment and location of the excited states are taken from Hirst [18]. Fifteen of these states can be populated at 0 eV, with the two lowest states quasidegenerate in energy. These are $X\ ^1\Sigma^+$, $a\ ^3\Pi$ (0.08 eV), $A\ ^1\Pi$ (1.03 eV), $b\ ^3\Sigma^-$ (1.09 eV), $c\ ^3\Sigma^+$ (1.36 eV), $B\ ^1\Delta$ (2.17 eV), $C\ ^1\Sigma^+$ (2.74 eV), $d\ ^3\Pi$ (3.52 eV), $^5\Pi$ (3.59 eV), $D\ ^1\Sigma^-$ (4.03 eV), $e\ ^3\Pi$ (5.11 eV), $f\ ^3\Delta$ (5.62 eV), $E\ ^1\Pi$ (5.87 eV), $F\ ^1\Sigma^+$ (5.87 eV), and $g\ ^3\Phi$ (5.88 eV).

In a similar manner, thirteen states—adapted from Honjou [19]—can be reached in the CO^+ production: $X\ ^2\Sigma^+$, $A\ ^2\Pi$ (2.83 eV), $a\ ^4\Sigma^+$ (5.10 eV), $B\ ^2\Sigma^+$ (5.93 eV), $b\ ^4\Delta$ (6.72 eV), $C\ ^4\Pi$ (6.79 eV), $d\ ^4\Sigma^-$ (7.35 eV), $C\ ^2\Pi$ (8.19 eV), $D\ ^2\Sigma^-$ (8.25 eV), $E\ ^2\Delta$ (8.36 eV), $^6\Sigma^+$ (9.08 eV), $F\ ^2\Pi$ (9.24 eV), and $G\ ^2\Delta$ (9.27 eV). It is worth mentioning that for a given electronic state, the AI process populates any rovibrational level that is energetically accessible. Therefore, our measurements refer to integral AI cross sections for excited molecular ions.

The integral cross sections along the $C^-+(C^+,N^+,O^+)$ channels are displayed in Fig. 1 for the associative ionization as a function of the collision energy E, with the vertical error bars representing the statistical uncertainties. The cross sections for C^-+C^+ are larger than those for C^-+N^+, themselves larger than those for C^-+O^+, that is to say, cross sections of 400, 120, and 50 Å^2 at 10 meV, respectively. This being rather a coincidence, it is worth noticing that the same trend was observed along the $O^-+(C^+,N^+,O^+)$ sequence [7].

Would this mean that the associative ionization process is dominated by the cationic reactants? From a quantitative point of view, several parameters are indeed critical to the

efficiency of the AI process, such as the number and location of the molecular-cation electronic states with respect to the entrance channel.

A first key parameter concerns the energetics of the different reactions. The lowest reaction channels are listed, with the exception of $CN^+(^3\Pi)+e^-$ and $C^+(^2P)+N(^2D)+e^-$.

$$C^-(^4S)+C^+(^2P)(<6.5\ \text{eV}) \rightarrow C_2(X\ ^1\Sigma_g^+)+h\nu(16.30\ \text{eV}), \tag{2a}$$

$$C(^3P)+C(^3P)+10.00\ \text{eV}, \tag{2b}$$

$$C_2^+(X\ ^4\Sigma_g^-)+e^-+4.90\ \text{eV}, \tag{2c}$$

$$C(^3P)+C^+(^2P)+e^--1.26\ \text{eV}, \tag{2d}$$

$$C^-(^4S)+N^+(^3P)(<3.0\ \text{eV}) \rightarrow CN(X\ ^2\Sigma^+)+h\nu(20.98\ \text{eV}), \tag{3a}$$

$$C(^3P)+N(^4S)+13.27\ \text{eV}, \tag{3b}$$

$$CN^+(X\ ^1\Sigma^+)+e^-+6.99\ \text{eV}, \tag{3c}$$

$$CN^+(a\ ^3\Pi)+e^-+6.91\ \text{eV}, \tag{3d}$$

$$C^+(^2P)+N(^4S)+e^-+2.01\ \text{eV}, \tag{3e}$$

$$C^+(^2P)+N(^2D)+e^--0.37\ \text{eV}, \tag{3f}$$

$$C(^3P)+N^+(^3P)+e^--1.26\ \text{eV}, \tag{3g}$$

$$C^-(^4S)+O^+(^4S)(<5.0\ \text{eV}) \rightarrow CO(X\ ^1\Sigma^+)+h\nu(23.45\ \text{eV}), \tag{4a}$$

$$C(^3P)+O(^3P)+12.36\ \text{eV}, \tag{4b}$$

$$CO^+(X\ ^2\Sigma^+)+e^-+9.44\ \text{eV}, \tag{4c}$$

$$C^+(^2P)+O^-(^2P)+2.56\ \text{eV}, \tag{4d}$$

$$C^+(^2P)+O(^3P)+e^-+1.10\ \text{eV}, \tag{4e}$$

$$C(^3P)+O^+(^4S)+e^--1.26\ \text{eV}. \tag{4f}$$

The asymptotic limit of CO^+ $(X\ ^2\Sigma^+)$ is $C^+(^2P)+O(^3P)$, situated below the entrance channel. As a consequence, autoionization may take place in the vibrational continuum of the molecular ion, identified with channel (4e). For the C^-+N^+ case, the dissociation limits of the lowest electronic states of the product molecular ion, i.e., $^1\Sigma^+$ and $^3\Pi$, reactions (3c) and (3d), are located slightly above and below the entrance channel, as they correspond to the transfer-ionization channels (3e) and (3f), respectively. Hence this competition affects the AI yield in a stepwise manner, the ground-state dissociation being responsible for the wavy structure of the cross section around 0.4 eV, while the $^3\Pi$ contribution is already reduced at zero energy. A similar competing channel, detachment reaction (2d), affects the C^++C^- AI cross section above 1.8 eV.

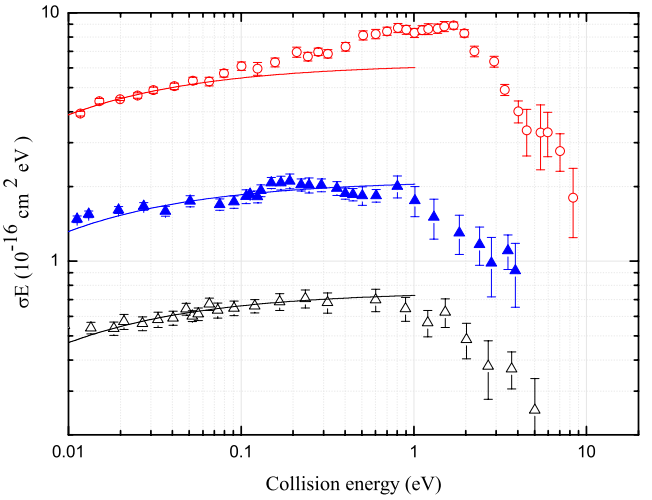

FIG. 2. (Color online) σE representation for the associative ionization process. Same symbols as in Figure 1.

The energy dependence of the cross sections is best seen in a reduced $\sigma \times E$ representation in Fig. 2. Below 0.1 eV, the cross-section curves follow the model cross section displayed in full lines corresponding to the pure Coulomb case, i.e., $\sigma \propto E^{-1}$. The departure at very low energy from a straight line obtained in the logarithmic representation is due to the finite resolution in our apparatus. Between 0.1 and 1.8 eV, an increase of the C^++C^- reduced cross section is observed. This departure from the E^{-1} dependence is interpreted as an increase in the number of rovibrational states accessed by autoionization, hence in the reaction probability. The observed energy shift, from 1.26 to 1.8 eV, has been explained by the population of rotationally excited states whose tunneling time through the centrifugal barrier greatly exceeds the time of flight to the detector. The absence of such a behavior in the C^-+N^+ and C^-+O^+ cases is consistent with the fact that all or most of the bound states of the molecular ion lie below the entrance channel asymptote, saturating the reaction probability at low energy. An additional consequence is that CN^+ and CO^+ products are formed with maximal rovibrational excitation, while C_2^+ ions are not.

The number of states of ionic nature that correlate to the entrance channel, their locations and subsequent curve crossings—with the cationic and covalent states—are also of prime importance. Since those are poorly characterized in the literature at any level of theory and even none at all, we have performed exploratory *ab initio* calculations in order to qualitatively describe the major pathways underlining our AI experiments.

Calculating all possible neutral and ionic electronic states correlating to the entrance and outgoing channels in an exhaustive way and the task of solving the nonadiabatic dynamics on the calculated potential energy curves is unfortunately too demanding, feasible only for few-electron systems. Such calculations should indeed consider the huge number of excited states arising from the highly degenerate

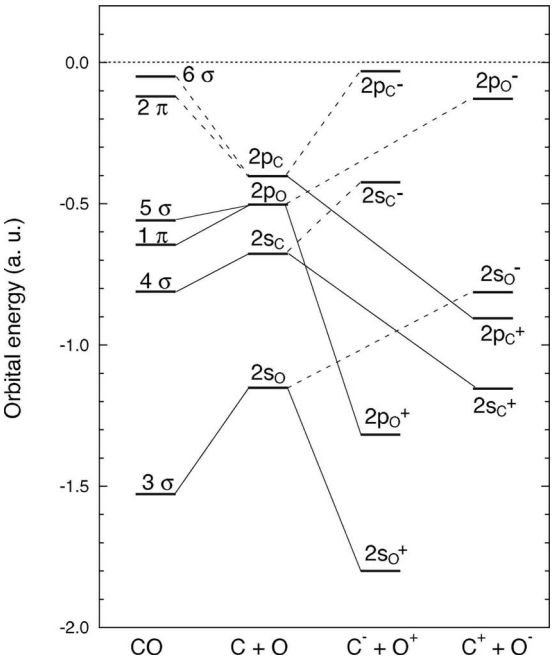

FIG. 3. Molecular orbital correlation diagram from CASSCF aug-ccpVTZ calculations. Full lines and dashed lines correspond to bonding and antibonding behavior with respect to the ground-state orbital energies of neutral atoms C and O.

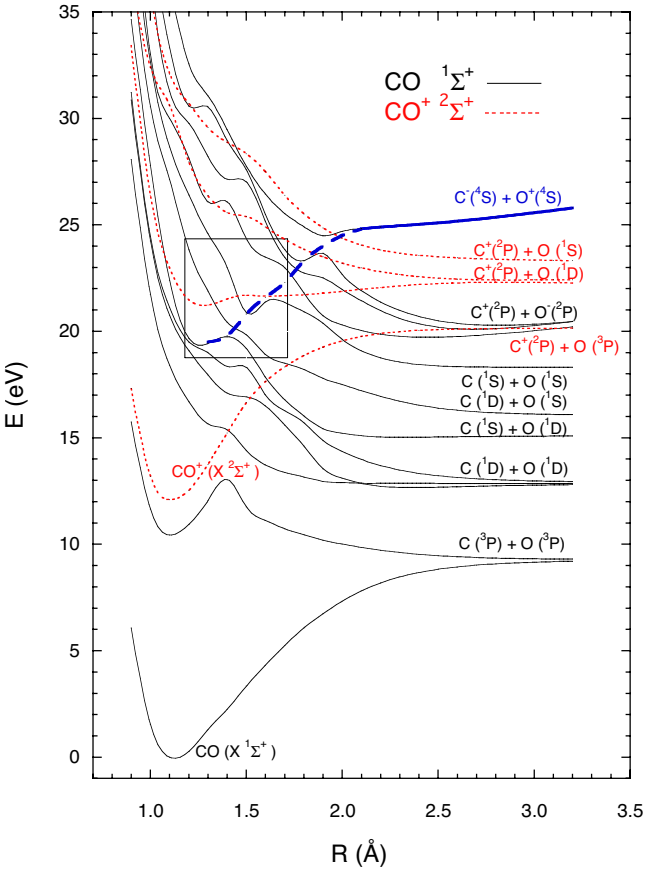

FIG. 4. (Color online) *Ab initio* CASSCF aug-ccpVTZ potential energy curves of Σ^+ symmetry of CO (full lines) and CO^+ (dotted lines). The diabatic pathway allowing the C^-+O^+ entrance channel to reach autoionization is shown by a bold dashed line. The rectangular box indicates the region where autoionization occurs.

dissociation channels. Furthermore, they should consider the difficult task of describing the strong electron correlation effects occurring in such a system, and the real challenge to reach the correct energy balance between neutral n-electron and ionic $(n+1)$-or $(n-1)$-correlated systems. In order to take such effects into account, we used variational multiconfigurational *ab initio* methods taking the full valence electron correlation into account.

For simplifying the problem, we decided to limit our calculations to the CO system, and to focus only on the states of $^1\Sigma^+$ symmetry for neutral CO and of $^2\Sigma^+$ symmetry for cationic CO^+. The goal of these calculations is to characterize the reactive pathways in this particular case. Calculations were performed with the MOLPRO quantum chemistry code [20] using the complete active space self-consistent field (CASSCF) approach [21] completed by pointwise multireference configuration interaction (MRCI) calculations [22]. Augmented polarized correlation consistent aug-ccp valence triple zeta (VTZ) [23] and aug-ccp valence 5 zeta (V5Z) [24] basis sets were employed for their completeness and flexibility, as shown in recent work on the isomerization process of neutral and cationic acetylene into vinylidene [25]. The advantage of such a multiconfigurational approach in which both orbitals and configuration mixing coefficients are variationally optimized is that it provides a deep analysis of the electronic changes occurring upon variation of the internuclear distance. The results are presented in Figs. 3 and 4.

The simple one-electron picture of the reaction partners is first depicted in Fig. 3, in the form of a molecular orbital (MO) correlation diagram. It tells us, as explained in textbooks, that forming CO from neutral atoms implies a stabilization of MOs 1σ to 5σ and 1π, which are bonding MOs, while 2π and 6σ are the antibonding counterparts of 5σ and 1π. This explains the stability of the $^1\Sigma^+$ ground state of CO arising from the closed-shell ground configuration. It also explains why the spectroscopic evidence [26] points to only a few excited valence states at energies above 6 eV from the ground state, that arise from singly excited configurations from 5σ and 1π to 2π. Another interesting point is the stabilization (destabilization) of the $2s$ and $2p$ atomic orbitals upon positive (negative) ionization, these effects being substantially more pronounced for the pair C^-+O^+ than for O^-+C^+. Figure 4 displays the CASSCF aug-ccpVTZ adiabatic potential energy curves corresponding to the 12 lowest $^1\Sigma^+$ states of CO (full lines) and the four lowest $^2\Sigma^+$ states of CO^+ (dotted lines). States correlating to the low-lying neutral and ionic dissociation channels are also represented. The two higher-energy curves of neutral CO dissociate to the first $C^+(^2P)+O^-(^2P)$ and $C^-(^4S)$ and $O^+(^4S)$ ionic channels, respectively. Since the relative energies are already of reasonable accuracy at the CASSCF level of theory, we only checked by pointwise MRCI calculations that dynamical correlation improves these energies, but does not change significantly the global shape of the potential curves and the electronic content of the wave functions. An extension of the basis set to aug-ccpV5Z was also tested, but it does not

change the latter conclusions. We thus believe that the picture provided in Fig. 4 is relevant for discussing AI pathways. Numerous avoided crossings clearly appear and nonadiabatic coupling is expected to play a decisive role in the reaction dynamics. Of particular interest is the C^-+O^+ entrance channel (in boldface on the figure), exhibiting a stabilizing diabatic trip across the lower-lying states, as depicted by the bold dashed line. One expects that a wave packet following this descending path will cross the energy region where it can mix with the continuum states of the molecular ionic species. Autoionization is thus expected to take place in the region marked by a rectangular box in the figure. A complete analysis of the CASSCF wave functions has been undertaken in order to interpret this process in terms of configuration changes. It shows that the entrance $C^-(^4S)$ and $O^+(^4S)$ channel diabatically crosses the lower curves with a progressive admixture of a configuration corresponding to a diexcitation from $5\sigma\,1\pi$ to $6\sigma\,2\pi$ applied to the ground-state configuration. This configuration becomes dominant in the eighth neutral state around 1.5 Å and in the sixth one around 1.2 Å. Analyzing the MOs and calculating the electron atomic populations tells us that this configuration corresponds to an ionic C^-+O^+ electronic structure. The stabilization of this structure promoting autoionization can be explained by the enhancement of the stability of the inner shells (3σ, 4σ, and 1π correlating to $2s$ and $2p$ of O^+, as shown in Fig. 3) when going from C+O to C^-+O^+. The above discussion is of course restricted to a single symmetry species of CO and CO^+. The calculations should be repeated for all possible space and spin symmetries arising from the considered dissociation limits. Such calculations, not performed in the present work, would provide a large number of potential energy curves that should be superimposed to those of Fig. 4 for getting the overall energy landscape governing the dynamics. We believe that such a complete description that would require large amounts of computer time is not necessary for predicting the possible autoionization pathways. One can indeed predict that similar crossing channels should occur in other symmetries and that the dynamics will depend on the statistic of population of the contributing channels, as will be discussed now.

When colliding two atomic species with given spin states and angular momenta, a restricted set of total spin and Λ symmetries are populated. However, not all of them may lead to the formation of ground-state molecular ions upon ejection of an electron. A severe limiting factor of the total reaction probability arises from the statistical counting of contributing channels. As an example, $C^-(^4S)+O^+(^4S)$ collisions occur along Σ states only, with total spin 3, 2, 1 and 0, hence a total multiplicity of 16. On the other hand, the CO^+ ground state has $^2\Sigma$ symmetry, which together with the ejected electron allows for total spin 1 or 0. Hence, only 4/16 of the collisions can possibly contribute to AI. Table I lists all ion-pair combinations and corresponding total-spin S values, together with spin states allowed to autoionize to ground-state ions. We ignore the distinction of Λ symmetries as this quantum number may be carried away by the departing electron.

For CN^+, the inclusion of the low-lying $^3\Pi$ state increases the number of efficient channels from 1/6 to 1/2. With this provision, the statistical treatment yields the correct ordering of the cross sections, i.e., $1:\frac{1}{2}:\frac{1}{4}$ for C^+, N^+, and O^+, respectively. The same statistical argument, when applied to our previous study of $O^-+(C^+,N^+,O^+)$ collisions [7], gives $1:1:\frac{3}{8}$ for C^+, N^+, and O^+, respectively, when including the $a\ ^3\Sigma^+$ state of NO^+, to be compared with the values measured at 10 meV, 370:240:80 Å^2.

TABLE I. Allowed spin symmetries in the entrance and exit channels, for C^- and O^- AI reactions with C^+, N^+ and O^+.

	$^{2s_1+1}L_1+^{2s_2+1}L_2$	S	$^{2s+1}\Lambda$	$s\pm 1/2$
C^-+C^+	$^4S+^2P$	1, 2	$^4\Sigma$	1, 2
C^-+N^+	$^4S+^3P$	$\frac{1}{2}, \frac{3}{2}, \frac{5}{2}$	$^1\Sigma$	$\frac{1}{2}$
			$^3\Pi$	$\frac{1}{2}, \frac{3}{2}$
C^-+O^+	$^4S+^4S$	0, 1, 2, 3	$^2\Sigma$	0, 1
O^-+C^+	$^2P+^2P$	0, 1	$^2\Sigma$	0, 1
O^-+N^+	$^2P+^3P$	$\frac{1}{2}, \frac{3}{2}$	$^1\Sigma$	$\frac{1}{2}$
			$^3\Sigma$	$\frac{1}{2}, \frac{3}{2}$
O^-+O^+	$^2P+^4S$	1, 2	$^2\Pi$	0, 1

The efficiency of the AI process has also to be discussed in terms of an interplay with other competing processes, and among them the very effective and always open mutual-neutralization (MN) process. We do not discuss the negligible contribution of the radiative association process, i.e., channels (2a), (3a), and (4a). The evaluation of the number of covalent pairs that sit below each of the three ionic entrance channels gives an estimate of the associating flux that goes to the MN, a flux which is therefore not available to leak into AI channels. There are 144 of these pairs between $C^+(^2P)+C^-(^4S)$ and $C(^3P)+C(^3P)$, i.e., within a 10 eV energy gap. The corresponding numbers are 1434 and 1031 between the $C^-(^4S)+N^+(^3P)$ to $C(^3P)+N(^4S)$ and $C^-(^4S)+O^+(^4S)$ to $C(^3P)+O(^3P)$ pairs, respectively—energy gaps of 13.27 and 12.36 eV. It follows that the MN process takes a much larger flux in the association along the C^-+N^+ and C^-+O^+ channels than in the C^-+C^+ case. As a consequence, this gives more flux and therefore more probability for the associative ionization to occur along the C^-+C^+ channel, corroborating the other observations.

We shall now compare the C^-+O^+ and O^-+C^+ channels whose respective AI processes are displayed in Fig. 5. Within the energy range under consideration, the situation for the O^-+C^+ channel is the following:

$$O^-(^2P)+C^+(^2P)(<14.0\ \text{eV}) \rightarrow CO(X\ ^1\Sigma^+)+h\nu(20.89\ \text{eV}), \tag{5a}$$

$$C(^3P)+O(^3P)+9.80\ \text{eV}, \tag{5b}$$

$$CO^+(X\ ^2\Sigma^+)+e^-+6.88\ \text{eV}, \tag{5c}$$

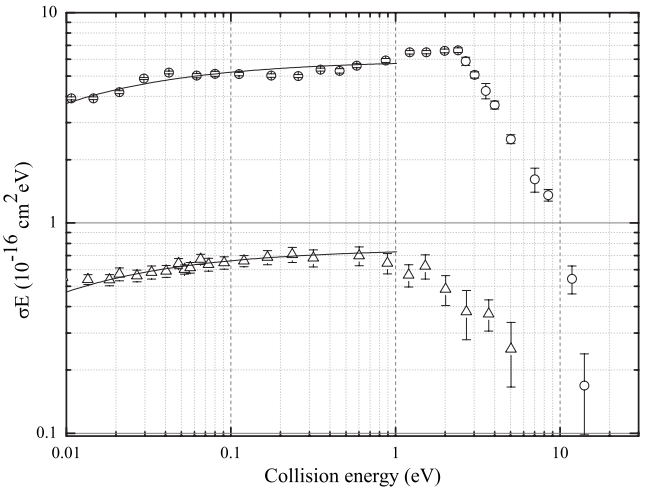

FIG. 5. σE representation for the associative ionization cross section along the O^-+C^+ channel (open circles) from [7], and along the C^-+O^+ channel (open triangles).

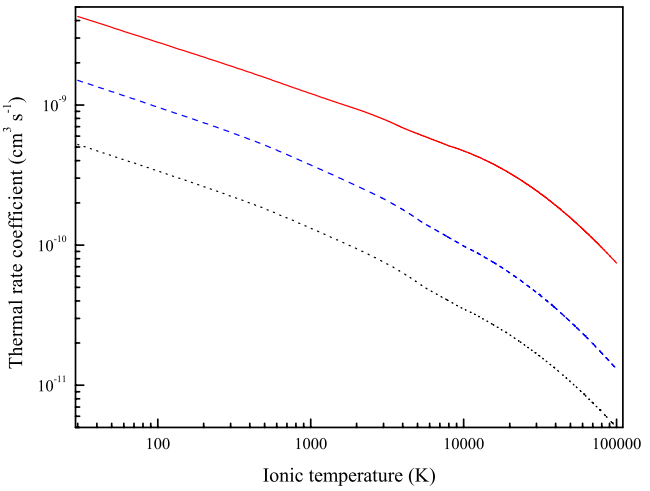

FIG. 6. (Color online)Thermal rate coefficients for the associative ionization as a function of the ionic temperature. The full line is for the association along the C^-+C^+ channel, the dashed line for the C^-+N^+ channel and the dotted line for the C^-+O^+ channel.

$$C^+(^2P) + O(^3P) + e^- - 1.46\ \text{eV}, \tag{5d}$$

$$C^-(^4S) + O^+(^4S) - 2.56\ \text{eV}, \tag{5e}$$

$$C(^3P) + O^+(^4S) + e^- - 3.82\ \text{eV}. \tag{5f}$$

The two AI channels lead to the very same molecular ion CO^+, not necessarily produced with the same internal excitation. We recall first a few points of discussion that are relative to the O^-+C^+ channel (see Ref. [7] for details). Between 0.04 and 1 eV, only a structureless E^{-1} energy dependence was seen, as well as a weak positive signal on top of this dependence above 1 eV. Some extra signal, due to the increasing number of accessible rovibrational levels in CO^+, is present in the O^-+C^+ case but not in the C^-+O^+ case. This is a result of all bound rovibrational levels of CO^+ being accessible at zero collision energy.

Considering the comparison of the AI efficiencies between the C^-+O^+ and O^-+C^+ channels, the AI cross sections for the latter one are much larger ($\sim$370 Å^2 at 10 meV) than those found for the former ($\sim$50 Å^2 at 10 meV). The substantial reduction of the cross section in the C^-+O^+ case demonstrates the strong competition exerted by the transfer-ionization channel, C^++O. This two-electron process seems unlikely to compete with AI. One must, however, recognize it as the vibrational continuum of the CO^+ ground electronic state to which autoionization takes place quite efficiently above the CO^+ dissociation limit. One additional fact may be responsible for the experimental findings. Keeping in mind that the $C^-(^4S)+O^+(^4S)$ asymptote sits 2.56 eV above the $O^-(^2P)+C^+(^2P)$ limit, the states converging to $C^-(^4S)+O^+(^4S)$ cross many more covalent C+O states than those arising from the $O^-(^2P)+C^+(^2P)$ pair, with the net effect of favoring the mutual neutralization in the C^-+O^+ case and subsequently hindering the corresponding associative ionization process.

For the sake of completeness, it should be pointed out that a similar finding was made with the D^-+O^+ and O^-+D^+ pairs [27] separated by 0.72 eV, the former pair being the higher in energy and displaying the lower AI efficiency, and vice versa. It also happens that the ratio $\sigma[O^-+D^+]/\sigma[D^-+O^+]$ over the energy gap of 0.72 eV matches perfectly that of $\sigma[O^-+C^+]/\sigma[C^-+O^+]$ over the energy gap of 2.56 eV for the pairs under scrutiny, though we consider that this is a coincidence. Though this has to be considered cautiously, a positive consequence of all of this would be the establishment of a scaling law, transposable to other ion-pair systems.

Since the associative-ionization thermal rate coefficients might be of some interest in plasma modeling, Fig. 6 displays them for the C^-+C^+, C^-+N^+, and C^-+O^+ pairs. These are obtained by folding the measured cross sections with a Maxwell-Boltzmann distribution, with the parameter μ standing for the reduced mass of the colliding system.

$$\alpha(T) = \frac{8\pi\mu}{(2\pi\mu k_B T)^{3/2}} \int_0^\infty \sigma(E) E \exp(-E/k_B T) dE. \tag{6}$$

One obtains rate values of 4.3, 1.5, and 0.5×10^{-9} cm^3 s^{-1} at 30 K, for the production of C_2^+, CN^+, and CO^+, respectively.

IV. CONCLUSION

This paper describes results that deal with the associative ionization along the $C^-+(C^+,N^+,O^+)$ channels. The three sets of measured integral cross-section curves point out a quite efficient process since we have measured 400, 120, and 50 Å^2 at 10 meV, from the C^-+C^+, C^-+N^+, and C^-+O^+ channels, respectively. The efficiencies were discussed in terms of spin statistics, and one may reproduce the observed ordering of the cross section by assuming substantial population of triplet states when N^+ is involved as a collision partner. We identified the interplay with other nonassociating channels that take a substantial part of the overall flux, namely, transfer ionization and collisional detachment, and the very efficient long-range mutual-neutralization process.

From energetic considerations, we have shown that the C_2^+ ions are produced with less internal energy than the CN^+ and CO^+ ions. We have also compared the production of CO^+ ions from the O^-+C^+ and C^-+O^+ pairs, and have found that the O^-+C^+ channel produces CO^+ ions colder than those from the C^-+O^+ channel. The major reactive pathway of the CO system has been characterized by means of an orbital correlation diagram and by quantum *ab initio* calculations of the low-lying potential energy curves of the neutral and cationic systems. We have shown that the entrance C^-+O^+ channel is diabatically crossing the lower-lying states, populated so a doubly excited configuration makes autoionization possible. Last, assuming a Maxwell-Boltzmann distribution, we deduced thermal rate coefficients from our data that are useful to model plasmas.

ACKNOWLEDGMENTS

This work was funded by the Belgian National Fund for Scientific Research (F.R.S.-FNRS) and the Euratom-Belgian state association. J.L. thanks the "Action de Recherches Concertées de la Communauté française de Belgique" for financial support. The authors would also like to thank Professon Colin Marsden for valuable comments on the manuscript.

[1] J. A. D. Pacheco, S. J. C. Landaberry, and P. D. Singh, Mon. Not. R. Astron. Soc. **235**, 457 (1988).
[2] D. L. Lambert, Y. Sheffer, and S. R. Federman, Astrophys. J. **438**, 740 (1995).
[3] J. H. Goebel, J. D. Bregman, D. M. Cooper, D. Goorvitch, S. R. Langhoff, and F. C. Witteborn, Astrophys. J. **270**, 190 (1983).
[4] W. S. Adams, Astrophys. J. **93**, 11 (1941).
[5] N. R. Erickson, R. L. Snell, R. B. Loren, L. Mundy, and R. L. Plambeck, Astrophys. J. **245**, L83 (1981).
[6] H. Storzer, J. Stutzki, and A. Sternberg, Astron. Astrophys. **296**, L9 (1995).
[7] T. Nzeyimana, E. A. Naji, X. Urbain, and A. Le Padellec, Eur. Phys. J. D **19**, 315 (2002).
[8] J. M. Ajello, J. Chem. Phys. **55**, 3158 (1971).
[9] M. F. A. Harrison, K. Dolder, and P. C. Thonemann, Proc. Phys. Soc. London, **82**, 368 (1963).
[10] M. Hamdan and A. G. Brenton, J. Phys. B **22**, 2289 (1989).
[11] M. Scheer, R. C. Bilodeau, C. A. Brodie, and H. K. Haugen, Phys. Rev. A **58**, 2844 (1998).
[12] D. Feldmann, Chem. Phys. Lett. **47**, 338 (1977).
[13] B. D. Rehfuss, D. J. Liu, B. M. Dinelli, M. F. Jagod, W. C. Ho, M. W. Crofton, and T. Oka, J. Chem. Phys. **89**, 129 (1988).
[14] P. Rosmus, H. J. Werner, E. A. Reinsch, and M. Larsson, J. Electron Spectrosc. Relat. Phenom. **41**, 289 (1986).
[15] K. Boudjarane, M. Carre, and M. Larzilliere, Chem. Phys. Lett. **243**, 571 (1995).
[16] P. J. Bruna and J. S. Wright, J. Phys. Chem. **96**, 1630 (1992).
[17] J. P. Maier and M. Rosslein, J. Chem. Phys. **88**, 4614 (1988).
[18] D. M. Hirst, Mol. Phys. **82**, 359 (1994).
[19] N. Honjou and F. Sasaki, Mol. Phys. **37**, 1593 (1979).
[20] MOLPRO 2006 is a package of *ab initio* programs written by H.-J. Werner, P. J. Knowles, R. Lindh, F. R. Manby, M. Schütz, P. Celani, T. Korona, G. Rauhut, R. D. Amos, A. Bernhardsson, A. Berning, D. L. Cooper, M. J. O. Deegan, A. J. Dobbyn, F. Eckert, C. Hampel, G. Hetzer, A. W. Lloyd, S. J. McNicholas, W. Meyer, M. E. Mura, A. Nicklass, P. Palmieri, R. Pitzer, U. Schumann, H. Stoll, R. Tarroni, and T. Thorsteinsson.
[21] H.-J. Werner and P. J. Knowles, J. Chem. Phys. **89**, 5803 (1988).
[22] H.-J. Werner and P. J. Knowles, J. Chem. Phys. **82**, 5053 (1985).
[23] T. H. J. Dunning, Jr., Chem. Phys. **90**, 1007 (1989).
[24] R. A. Kendall, T. H. Dunning, and R. J. J. Harrison, Chem. Phys. **96**, 6796 (1992).
[25] S. Boyé-Péronne, D. Gauyacq, and J. Liévin, J. Chem. Phys. **124**, 214305 (2006).
[26] K. P. Huber and G. Herzberg *Molecular Spectra and Molecular Structure. IV. Constants of Diatomic molecules* Van Nostrand Reinhold, (New York, 1979).
[27] E. A. Naji, T. Nzeyimana, X. Urbain, and A. Le Padellec, J. Phys. B **35**, 4325 (2002).